

BCTR: Bidirectional Conditioning Transformer for Scene Graph Generation

Peng Hao, Xiaobing Wang, Yingying Jiang, Hanchao Jia, Xiaoshuai Hao

Samsung R&D Institute China-Beijing
 {peng1.hao, x0106.wang, yy.jiang, hanchao.jia, xiaoshuai.hao}@samsung.com

Abstract

Scene Graph Generation (SGG) remains a challenging task due to its compositional property. Previous approaches improve prediction efficiency by learning in an end-to-end manner. However, these methods exhibit limited performance as they assume unidirectional conditioning between entities and predicates, leading to insufficient information interaction. To address this limitation, we propose a novel bidirectional conditioning factorization for SGG, introducing efficient interaction between entities and predicates. Specifically, we develop an end-to-end scene graph generation model, Bidirectional Conditioning Transformer (BCTR), to implement our factorization. BCTR consists of two key modules. First, the Bidirectional Conditioning Generator (BCG) facilitates multi-stage interactive feature augmentation between entities and predicates, enabling mutual benefits between the two predictions. Second, Random Feature Alignment (RFA) regularizes the feature space by distilling multi-modal knowledge from pre-trained models, enhancing BCTR’s ability on tailed categories without relying on statistical priors. We conduct a series of experiments on Visual Genome and Open Image V6, demonstrating that BCTR achieves state-of-the-art performance on both benchmarks. The code will be available upon acceptance of the paper.

Introduction

Scene Graph Generation (SGG) aims to endow computers with the ability to comprehend scenes by detecting objects and identifying relationships within an image. This process generates structured relationships in the form of triplets (object-predicate-subject). SGG holds potential for a wide range of downstream applications, including question answering (Shi, Zhang, and Li 2019), image captioning (Yang et al. 2019), and image retrieval (Johnson et al. 2015).

Previous SGG studies can be categorized into two groups: two-stage and one-stage methods. Two-stage methods separate the SGG task into entity detection and predicate detection stages, often generating $O(N^2)$ relationship candidates and requiring significant computational resources. Inspired by fully convolutional one-stage object detection approaches (Carion et al. 2020; Sun et al. 2021), one-stage methods have been introduced to directly detect relationships from image features (Liu et al. 2021; Teng and Wang 2022), thereby enhancing detection efficiency by avoiding the requirement to consider all possible pairs. However, these methods lack ex-

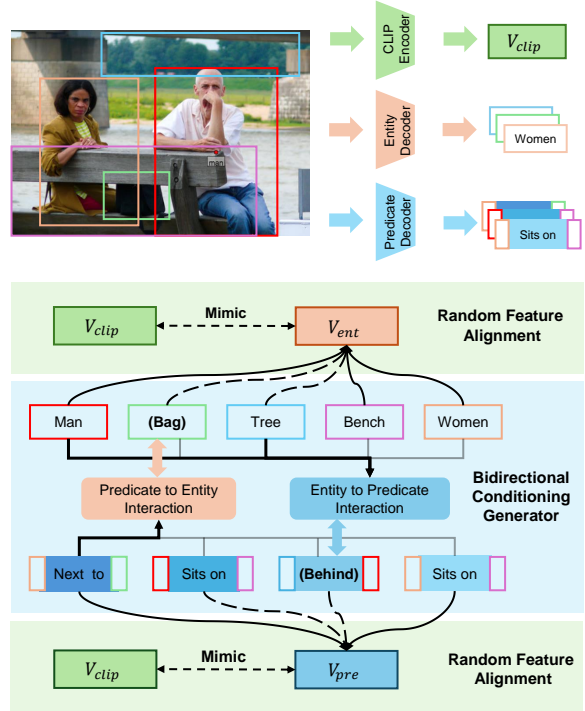


Figure 1: The illustration of the BCTR pipeline paradigm. The top part shows the extraction of CLIP, entity, and predicate features from the input image. The bottom part demonstrates how entity (e.g., Bag) and predicate detection (e.g., Behind) are enhanced through feature interaction via the proposed BCG. Additionally, the output features are regularized by RFA to mitigate the long-tail problem.

PLICIT entity modeling and struggle to capture complex relationships within images. To address this, recent one-stage methods (Li, Zhang, and He 2022; Shit et al. 2022) have conditioned predicate prediction on entity features to improve task performance. Nevertheless, this fixed unidirectional dependence often yields suboptimal results, as entity detection cannot benefit from predicate detection within their pipelines. Moreover, current one-stage methods fail to explicitly address the long-tail distribution (Kundu and Aakur 2023), resulting in biased predictions.

To address these limitations, we propose a novel bidirectional conditioning factorization for SGG, introducing efficient interaction between entities and predicates. Technically, we develop a one-stage SGG model to implement our factorization, dubbed Bidirectional Conditioning TRansformer (BCTR). The overview of BCTR is shown in Fig. 1, consisting of two modules. The Bidirectional Conditioning Generator (BCG) is introduced to establish mutual dependencies between the entity and predicate decoders through two feature interaction mechanisms. The inner interaction uses Bidirectional Attentions (BiAtt) to enhance information exchange between entities and predicates, while the outer interaction employs iterative refinement to condition current detections on previous estimates, further improving the interaction between the two predictions. Additionally, Random Feature Alignment (RFA) is designed to address the long-tail problem without relying on the statistical priors of datasets. By randomly distilling knowledge from Vision-Language Pre-trained Models (VLPMS), RFA aligns the feature spaces of entity and predicate decoders with the VLPMS while preserving diversity for SGG tasks. Collaborating with CLIP-based classifiers, RFA boosts BCTR’s performance for tail classes and unseen relations. We validate the proposed method on two representative SGG datasets: Visual Genome and Open Image V6. Experimental results demonstrate that BCTR achieves superior performance on both benchmarks compared to existing methods. Our contributions can be summarized as follows:

- We propose a novel bidirectional conditioning factorization for SGG, enhancing the information exchange between predicates and entities by introducing mutual dependence.
- We develop an end-to-end SGG model BCTR to implement our factorization. Specifically, BCG is designed to augment the feature spaces through a bidirectional attention mechanism.
- RFA is introduced to regularize the feature spaces with VLPMS while preserving diversity for downstream tasks. RFA improves BCTR’s performance on tail categories without relying on statistical priors.
- Extensive experiments on the Visual Genome and Open Image V6 datasets demonstrate that BCTR achieves state-of-the-art performance compared to baselines.

Related Work

Conditional Dependencies in SGG One-stage SGG methods (Liu et al. 2021; Teng and Wang 2022) directly detect predicates or relationships from image features, avoiding time-consuming combinations. Inspired by one-stage detection methods (Sun et al. 2021; Carion et al. 2020), previous works have designed Relation Affinity Fields (Liu et al. 2021) or used query-based detection (Teng and Wang 2022) for one-stage SGG. However, these methods demonstrate poor performance as they do not utilize entity detection information (Li, Zhang, and He 2022). Recent studies (Li, Zhang, and He 2022; Shit et al. 2022; Cong, Yang, and Rosenhahn 2023; He et al. 2023) have explicitly incorporated entity features into relationship detection to im-

prove the performance of one-stage SGG. Nevertheless, these methods either condition predicates on entities (Li, Zhang, and He 2022; Shit et al. 2022) or condition entities on predicates (Desai et al. 2022), creating unidirectional dependencies that limit feature interactions and thus show limited performance.

Khandelwal et al. (Khandelwal and Sigal 2022) argue that SGG performance can benefit from dynamic conditioning on the image. By implicitly using a joint loss and explicitly through cross-decoder interactions, predictions are effectively refined from previous estimates. However, their predicate is still unidirectionally conditioned on the entity in each inner round, indicating that their dynamic conditioning is implemented mainly through iterative refinement. Their experimental results show that their network architecture offers minimal improvement to the task. In contrast to previous works, we propose the BCG to provide internal bidirectional dependencies, strengthening the features in each step. BCG offers flexible mutual dependence for the SGG task without altering the loss function.

Message Passing in SGG Message passing aims to increase prediction performance through information interaction between individual predictions and the surrounding context. Zhu et al. (Zhu et al. 2022) categorize them into local message passing within a triplet and global message passing across all elements. They point out that different prediction structures have variable ranges during message passing. Triplet set-based methods (Li et al. 2017; Yin et al. 2018) generally rely on local message passing, while chain (Xu et al. 2017), tree (Tang et al. 2019), and fully-connected graph (Li et al. 2021) methods usually achieve global message passing. Compared to local message passing, global message passing can resolve ambiguities of local predictions by integrating contextual information. Unlike previous works, we design the BiAtt-based BCG to enable global message passing within the set structure. Compared to previous works that rely on local explicit edges for propagation, BCG employs implicit global connections for more efficient information exchange.

Language Prior for Long-Tail Problem The long-tail distribution presents a significant challenge in SGG (Zhu et al. 2022). The community has developed numerous unbiased SGG methods, with re-balancing (Desai et al. 2021; Li et al. 2021) being one widely used approach. However, these methods are limited in open-set tasks due to their reliance on the statistical prior of the dataset. Chang et al. (Chang et al. 2021) argue that the long-tail problem can be addressed with language priors. Lu et al. (Lu et al. 2016) use a language prior module that projects semantic-like relationships into a compact embedding space, enabling the model to infer similar visual relationships. Their work demonstrates the potential of solving the long-tail problem by aligning the image and language spaces. However, the performance of language priors-based methods is affected by the poor alignment of multi-modal features.

Recently, VLPMS have made breakthroughs in multi-modal tasks (Gan et al. 2022). A series of VLPMS have achieved superior performance in aligning image and language features. By distilling features from VLPMS, down-

stream classifiers can recognize more objects and improve detection results on tail categories (Liao et al. 2022; He et al. 2023). However, research on using language prior to one-stage SGG is still lacking, and current methods fail to explicitly address the long-tail distribution (Kundu and Aakur 2023). Motivated by this, we propose RFA, which aligns the visual feature space of SGG with pre-trained language space to solve the long-tail problem. To the best of our knowledge, RFA is the first method to use a multi-modal model to address data imbalance in SGG, suggesting a potential impact for open-set relation detection.

External Knowledge in SGG Enhancing SGG performance with external knowledge is a crucial research direction (Zhu et al. 2022). Previous SGG works (Yu et al. 2017; Kim et al. 2024) usually extract statistical information from external textual knowledge (e.g., Wikipedia, ConceptNet). However, statistical information such as co-occurrence frequency is limited in revealing the complex, structured patterns of commonsense, which may lead to poor learning improvement (Lin, Zhu, and Liang 2022). Generally, using external knowledge to guide feature refinement is another effective approach. Gu et al. (Gu et al. 2019) proposed a knowledge-based module that improves the feature refinement procedure by reasoning over a collection of commonsense knowledge retrieved from ConceptNet. Zhan et al. (Zhan et al. 2019) introduced a novel multi-modal feature-based undetermined relationship learning network. Unfortunately, Zareian et al. (Zareian et al. 2020) point out that incomplete and inaccurate external commonsense tends to limit task performance. Unlike previous works, BCTR uses pre-trained multi-modal models as a source of external knowledge. By embedding knowledge through feature distillation, the model can learn better feature representations for SGG, thereby exhibiting superior ability on complex and unseen relationships.

Problem Formulation

SGG aims to detect objects and predicates from input images and represent them as a scene graph $\mathcal{G} = \{\mathcal{V}, \mathcal{E}\}$, where \mathcal{V} and \mathcal{E} denote the sets of vertices and edges, respectively. Specifically, \mathcal{V} includes all detected objects in the image, while \mathcal{E} comprises the predicates between object pairs. The categories of objects and predicates are defined by the task dataset.

Previous one-stage SGG methods typically assume a unidirectional information flow, such as $I \rightarrow s, o \rightarrow p$ (Li, Zhang, and He 2022; Cong, Yang, and Rosenhahn 2023), or $I \rightarrow p \rightarrow s, o$ (Desai et al. 2022), limiting mutual benefits between the two predictions. Teng et al. (Teng and Wang 2022) formulated SGG as $I \rightarrow p, s, o$ to facilitate feature interaction. However, the huge compositional triplet space is challenging to optimize. This paper proposes a novel factorization for SGG, as shown in Eq. 1. The first term reflects $I \rightarrow s, o$ and $I \rightarrow p$, avoiding the problem of large compositional space. The second term ensures bidirectional independence of $p \leftrightarrow s, o$, allowing the two predictions to benefit from each other.

$$Pr(E, P|I) = Pr(\hat{E}, \tilde{P}|I) \cdot Pr(E, P|\hat{E}, \tilde{P}). \quad (1)$$

Following previous work (Li, Zhang, and He 2022), we formulate SGG as a bipartite graph construction task. Specifically, the SGG model independently outputs predictions of entities and predicates from image features, forming two node sets \mathcal{V}_e and \mathcal{V}_p . Two directional edge sets \mathcal{E}_{ep} and \mathcal{E}_{pe} connect these node sets, representing the direction from entities to predicates and vice versa. The bipartite graph is then represented as $\mathcal{G}_b = \{\mathcal{V}_e, \mathcal{V}_p, \mathcal{E}_{ep}, \mathcal{E}_{pe}\}$, from which the scene graph of the image can be extracted.

Method

This section presents BCTR for implementing the factorization in Eq. 1, as illustrated in Fig. 2. First, we introduce feature extraction using the backbone. Next, we detail BCG, which provides mutual dependence for entity and predicate detection through BiAtt. RFA is then introduced to enhance performance for long-tail distributions by randomly distilling knowledge from CLIP. Then, we describe graph assembling, aiming to construct the scene graph from entity and predicate results. Finally, model training and inference are detailed.

Feature Extraction

Inspired by the previous one-stage detection method DETR (Carion et al. 2020), we utilize a CNN and Transformer to extract features $V \in \mathbb{R}^{w \times h \times c}$ from the input image I , where w , h , and c represent the width, height, and channel of the features, respectively. As previous one-stage SGG methods have shown that models struggle to directly capture predicates from image features without using intermediate information (e.g., entity features), we further extract entity features $V_e \in \mathbb{R}^{N_e \times c}$ from V as auxiliary features, as shown in the following:

$$V_e = f_e(V, Q_e), \quad (2)$$

where $f_e, Q_e \in \mathbb{R}^{N_e \times c}$ represent the transformer-based decoder and the learnable queries, respectively, with N_e denoting the number of queries.

Bidirectional Conditioning Generator

This subsection provides details of the Bidirectional Conditioning Generator, as illustrated in Fig. 2. BCG comprises two interactive branches that take visual features V as input and output augmented entity features and compositional predicate features, respectively. To improve performance, we introduce the iterative improvement mechanism into BCG. Specifically, we factorize the conditional distribution of entity and predicate according to Eq. 1, which are as follows:

$$Pr(E^t|I, E^{t-1}, \tilde{P}^t) = Pr(\hat{E}^t|I, E^{t-1}) \cdot Pr(E^t|\hat{E}^t, \tilde{P}^t), \quad (3)$$

$$Pr(P^t|I, P^{t-1}, \hat{E}^t) = Pr(\tilde{P}^t|I, P^{t-1}, \hat{E}^t) \cdot Pr(P^t|\hat{E}^t, \tilde{P}^t), \quad (4)$$

where E^t and P^t represent the entity and predicate estimates at phase t , respectively, while $\tilde{\cdot}$ and $\hat{\cdot}$ denote the temporal estimates at each phase. The first terms of the two equations

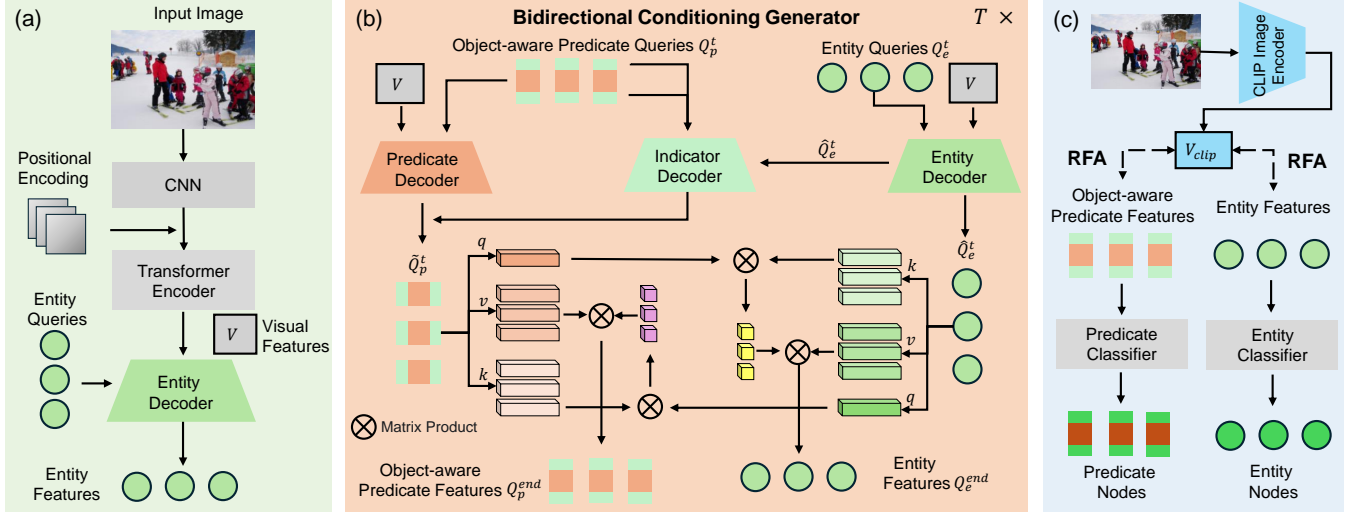


Figure 2: An illustration of the overall pipeline of BCTR: (a) Visual and entity features are extracted from the input image. (b) The compositional predicate and entity queries are iteratively updated through the proposed BCG. (c) The output features of various decoders are regularized by the RFA during training. The final predictions are derived from the distilled features.

predict the temporal estimates \tilde{P}^t and \hat{E}^t from the previous estimations and images, corresponding to the first term of Eq. 1. The second terms establish bidirectional dependencies between entities and predicates, corresponding to the second term of Eq. 1. The implementation details of Eq. 3 and Eq. 4 are introduced as follows.

Inspired by previous work (Li, Zhang, and He 2022) showing that predicate detection benefits from entity detection, we initialize Q_p^0 randomly to obtain the compositional predicate queries Q_{com}^{t-1} for the current scene, implemented as follows:

$$Q_{com}^{t-1} = A(q = Q_p^0, k = V_e, v = V_e), \quad (5)$$

where A denotes the attention block, where q, k, v represent the query, key, and value of the attention network, respectively. Q_{com}^{t-1} serves as the input to the predicate branch at phase t , consisting of three sub-queries: Q_{io}^{t-1} , Q_p^{t-1} , and Q_{is}^{t-1} . Q_e^{t-1} is the input to the entity branch at phase t , initialized from V_e . At each step t , Q_p^{t-1} and Q_e^{t-1} are updated with image features V via a cross-attention module, defined as follows:

$$\hat{Q}_e^t = A(q = Q_e^{t-1}, k = V, v = V), \quad (6)$$

$$\hat{Q}_p^t = A(q = Q_p^{t-1}, k = V, v = V). \quad (7)$$

The Eq. 6 corresponds to the first term of Eq. 3. Then, Q_{io}^{t-1} and Q_{is}^{t-1} are updated with entity features \hat{Q}_e^t through cross-attention. This step aims to identify the entity pairs that match the corresponding predicates from the current entity detection. The process is implemented as follows:

$$\hat{Q}_{io}^t = A(q = Q_{io}^t, k = \hat{V}_e^t, v = \hat{V}_e^t), \quad (8)$$

$$\hat{Q}_{is}^t = A(q = Q_{is}^t, k = \hat{V}_e^t, v = \hat{V}_e^t), \quad (9)$$

where $\hat{V}_e^t = V_e + \lambda \text{Norm}(\hat{Q}_e^t)$. After updating these queries with the corresponding decoder, \hat{Q}_p^t is further augmented with the updated indicator queries to adjust the predicate distribution, computed as follows:

$$\tilde{Q}_p^t = (\hat{Q}_p^t + (\hat{Q}_{io}^t + \hat{Q}_{is}^t) \cdot W_i) \cdot W_p. \quad (10)$$

Eq. 7 to Eq. 10 correspond to the first term of Eq. 4, where W_i and W_p represent transformation matrices. The indicator queries \hat{Q}_{io}^t and \hat{Q}_{is}^t are computed from entity features, enhancing the predicate query \tilde{Q}_p^t based on current entity detection. However, entity detection does not yet benefit from predicates. To address this, we propose a bidirectional attention module to establish conditional dependencies between entities and predicates, augmenting entity and predicate features mutually. This module is implemented as follows:

$$Q_e^t = A(q = \hat{Q}_e^t, k = \tilde{Q}_p^t, v = \tilde{Q}_p^t), \quad (11)$$

$$Q_p^t = A(q = \tilde{Q}_p^t, k = \hat{Q}_e^t, v = \hat{Q}_e^t). \quad (12)$$

Eq. 11 and Eq. 12 correspond to the second terms of Eq. 3 and 4, respectively. After the bidirectional interaction, the updated queries Q_p^t , \hat{Q}_{io}^t , \hat{Q}_{is}^t , and Q_e^t are used as inputs for the next phase. Through multi-stage iterative refinement, the bidirectional interaction between entities and predicates is further enhanced. At the end of the iterations, the final queries Q_{com}^{end} and Q_e^{end} are fed into the corresponding Multi-Layer Perceptrons (MLPs) to predict the entity and predicate distributions, respectively.

Random Feature Alignment

In this subsection, we introduce the details of Random Feature Alignment, illustrated in Fig. 3. RFA distills knowledge from a pre-train CLIP model, constraining the feature space

of various decoders aligned with CLIP. Furthermore, the parameters of the predicate and entity classifiers are initialized with the CLIP text encoder and fine-tuned on the SGG dataset. The specifics of feature distillation and classifier initialization are detailed as follows.

Random Feature Alignment SGG has suffered from the long-tail problem for a long time. Although previous studies have attempted to alleviate this issue by re-balancing the dataset distribution during training (Khandelwal and Sigal 2022; Li et al. 2021), the requirement for statistical prior limits its applicability in real-world settings.

To address this problem, we introduce the VLPMs to regularize the feature space of the SGG model and enhance its performance in modeling tail categories. Specifically, the input image is sent to the CLIP visual encoder to obtain V_{clip} . Since CLIP is trained with supervision from image captions, the encoder features V_{clip} are inclined to capture the gist of the image. However, images may contain various relationships. Simply aligning the decoder’s features Q_p^{end} and Q_e^{end} with CLIP may destroy the diversity of features. Therefore, we randomly select a portion of the decoder’s features before each alignment to ensure that the distilled features maintain diversity while being aligned with CLIP. The overall masked distillation process is as follows:

$$\mathcal{L}_{mimic} = \left| V_{clip} - \frac{1}{N_p} \sum_{i=1}^{N_p} \bar{Q}_p^{end} \right| + \left| V_{clip} - \frac{1}{N_e} \sum_{i=1}^{N_e} \bar{Q}_e^{end} \right|, \quad (13)$$

where \bar{Q}_p^{end} and \bar{Q}_e^{end} are randomly sampled from Q_p^{end} and Q_e^{end} , respectively. N_p and N_e denote the number of predicate and entity queries. An example is shown in Fig. 3. Taking $Q_p^{end} \in \mathbb{R}^{N_e \times c}$ as an example, the mask vectors $V_{mask} \in \mathbb{R}^{N_e \times 1}$ are generated with a mask ratio α . The values of V_{mask} are set to 0 with a probability of α , and the remaining values are set to $(1/(1-\alpha))$. Then, the dimensions of V_{mask} are expanded and multiplied with Q_p^{end} to obtain \bar{Q}_e^{end} . Finally, the mean feature of \bar{Q}_e^{end} is used to match the pre-trained features, as described in Eq. 13.

Through random sampling, some features are aligned with CLIP, while others capture content missing from the CLIP features. After training, the feature space of the decoders aligns with CLIP’s feature space, and multiple queries can capture the rich triplets in the image.

CLIP-based Classifier After feature distillation, the decoder features Q_p^{end} and Q_e^{end} are aligned with CLIP. To effectively utilize these features, we introduce classifiers based on CLIP text features. Specifically, we generate descriptions by replacing * in "A photo of a/an *" with the corresponding entity or predicate classes. These descriptions are then input to the CLIP text encoder to obtain the corresponding feature vectors. Finally, these generated vectors are used to initialize the parameters of the entity and predicate classifiers, respectively. During training, the two classifiers are fine-tuned with a smaller learning rate to further improve performance on the downstream datasets. The whole process is illustrated in Fig. 3.

Graph Assembling

Inspired by previous work (Li, Zhang, and He 2022), this section details the combination of predicted entity and

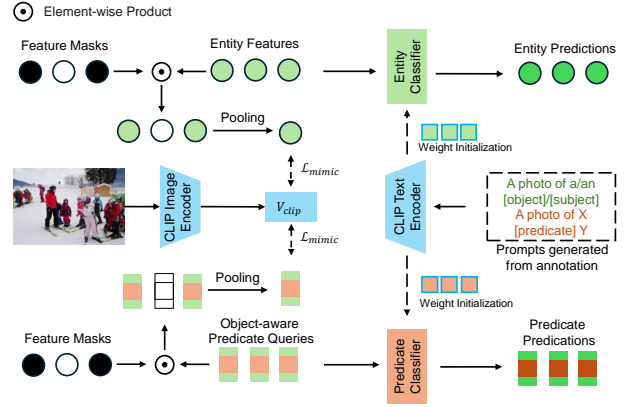


Figure 3: Random Feature Alignment for the entity and predicate prediction. First, the decoder feature is randomly distilled with the CLIP features of the input image. Then, the weights of the classifier are initialized with the vectors that are generated by the CLIP text decoder encoding the ground-truth, ensuring the aligned visual features can be correctly classified.

object-aware predicate nodes to generate triplets. Taking the connection of objects and predicates as an example, given the object node set N_o and the predicate node set N_p , we first obtain the adjacency matrix M_o , which indicates the distance between the corresponding nodes, calculated as follows:

$$M_o = d_{loc}(B_o, B_{po}) \cdot d_{cls}(P_o, P_{po}), \quad (14)$$

where d_{loc} and d_{cls} are the distance functions used to measure the matching quality in terms of bounding box locations and classes. B_o , B_{po} , P_o , and P_{po} are the bounding box predictions and classification distributions of objects and indicators of objects, respectively. Similarly, the adjacency matrix between objects and predicates M_s is calculated in the same manner. By selecting the top K relationships from the two matrices, the final predictions can be obtained in the form $T = \{(B_o, B_s, B_p, P_o, P_s, P_p)\}$. The details of graph generation are provided in the supplementary materials.

Training and Inference

Training To optimize the parameters of the proposed model, we design a multi-task loss function consisting of three components. \mathcal{L}_{ent} represents the loss for entity prediction, \mathcal{L}_{pre} is for predicate prediction, and \mathcal{L}_{mimic} is for feature distillation. The overall loss function is as follows:

$$\mathcal{L} = \mathcal{L}_{ent} + \mathcal{L}_{pre} + \mathcal{L}_{mimic}. \quad (15)$$

Since the entity detector follows a DETR-like architecture, \mathcal{L}_{ent} takes a similar form as described in (Carion et al. 2020). To calculate \mathcal{L}_{pre} , we first convert the ground-truth relationships in the image into the same form as predictions T , denoted as T_{gt} . Then, the Hungarian matching algorithm is used to measure the cost between the ground truth and

Table 1: The Results Comparison in Visual Genome

Method		mR@			R@			mR@100		
		20	50	100	20	50	100	Head	Body	Tail
two-stage	MOTIFS(Zellers et al. 2018)	4.2	5.7	-	21.4	27.2	-	-	-	-
	RelDN(Zhang et al. 2019)	-	6.0	7.3	-	31.4	35.9	-	-	-
	VCTree-TDE(Tang et al. 2020)	-	9.3	11.1	-	19.4	23.2	-	-	-
	BGNN(Li et al. 2021)	7.5	10.7	12.6	23.3	31.0	35.8	34.0	12.9	6.0
one-stage	FCSGG(Liu et al. 2021)	2.7	3.6	4.2	16.1	21.3	25.1	-	-	-
	SRCNN(Teng and Wang 2022)	6.2	8.6	10.3	26.1	33.5	38.4	-	-	-
	ISGG(Khandelwal and Sigal 2022)	-	8.0	8.8	-	29.7	32.1	31.7	9.0	1.4
	Relationformer(Shit et al. 2022)	4.6	9.3	10.7	22.2	28.4	31.3	-	-	-
	SGTR(Li, Zhang, and He 2022)	-	12.0	15.2	-	24.6	28.4	28.2	18.6	7.1
	RelTR(Cong, Yang, and Rosenhahn 2023)	6.8	10.8	12.6	21.2	27.5	-	30.6	14.4	5.0
	SG2HOI(He et al. 2023)	8.9	11.4	13.9	21.2	25.9	30.3	27.5	18.2	5.3
	DSGG(Hayder and He 2024)	-	13.0	17.3	-	32.9	38.5	-	-	-
	EGTR(Im et al. 2024)	5.5	7.9	10.1	23.5	30.2	34.3	-	-	-
	PGSG(Li et al. 2024)	-	10.5	12.7	-	20.3	23.6	-	-	-
	BCTR(ours)	8.1	13.7	18.4	20.1	24.8	27.7	27.7	22.0	11.9
one-stage statistical-based long-tail w/ strategy	ISGG+Rw(Khandelwal and Sigal 2022)	-	15.7	17.8	-	27.2	29.8	28.5	18.8	13.3
	SGTR+BiLvl(Li, Zhang, and He 2022)	-	15.8	20.1	-	20.6	25.0	21.7	21.6	17.1
	RelTR+LA(Cong, Yang, and Rosenhahn 2023)	9.7	14.2	-	19.8	25.9	-	28.3	19.4	10.2
	BCTR(ours)+LA	12.7	17.4	20.9	17.2	21.9	25.2	24.6	23.4	17.4

predictions, incorporating both predicate and entity information. The cost is computed as follows:

$$C = \lambda_p C_p + \lambda_e C_e, \quad (16)$$

where C_p and C_e represent the cost of the predicate and the entity, respectively. The matching results are obtained by selecting the minimum costs and are used to guide the calculation of \mathcal{L}_{pre} . Specifically, \mathcal{L}_{pre} consists of two parts: \mathcal{L}_{pre}^i and \mathcal{L}_{pre}^p , representing the losses for indicator and predicate predictions, respectively. Both \mathcal{L}_{pre}^i and \mathcal{L}_{pre}^p include losses for bounding box predictions \mathcal{L}_{box} (GIOU loss) and classification distributions \mathcal{L}_{cls} (cross-entropy loss). \mathcal{L}_{mimic} is implemented using the L1 loss function.

Inference During inference, the feature distillation module is removed as it only contributes during the training phase. After assembling the graph with predictions, $K \cdot N_p$ triplets are obtained. To obtain the final results, we first remove self-connected predictions, where the object and the subject of the triplets are identical. Then, by re-ranking all the triplets with the belief score S , the top K of them are selected as the final prediction results. The belief score S is the product of the classification probabilities of the corresponding subject entity, object entity, and predicate.

Experiments

Datasets We conduct evaluation experiments on two representative datasets, namely Visual Genome (Krishna et al. 2017) and Open Image V6 (Kuznetsova et al. 2020).

Evaluation Metrics The evaluation metrics are adopted from previous works (Xu et al. 2017; Tang et al. 2019). For Visual Genome, the mean Recall (mR@) represents the average recall across all classes. We also report Recall (R@) to reflect the model’s recall performance on all categories. Additionally, we report the mR@100 for each category group: head, body, and tail, to evaluate the model’s performance

on long-tail distribution. For Open Image V6, in addition to R@ and mR@, weighted metrics ($wmAP_{phr}$, $wmAP_{rel}$, $score_{wtd}$) are used for a more class-balanced evaluation.

Implementation Details We utilized ResNet-101 and DETR (Carion et al. 2020) as the feature extraction module. Additionally, the entity decoder shares the same architecture as the DETR decoder. To ensure training convergence, the model is initially trained with feature distillation without the entity branch. Subsequently, the entity branch is introduced into the iteration while the bidirectional attention is activated for joint training. The numbers of entity and predicate queries are set to 100 and 160, respectively, and the number of iterations (stages) is empirically set to 6. More details of parameter settings are reported in the supplementary materials.

Comparisons with State-of-the-Art Methods

Baselines As BCTR is a one-stage SGG method, we primarily compare it with current one-stage SGG methods, which are mainly based on transformers (Li, Zhang, and He 2022; Khandelwal and Sigal 2022; Cong, Yang, and Rosenhahn 2023; Shit et al. 2022; He et al. 2023). Additionally, we also compare our method with some representative two-stage methods (Li et al. 2021; Tang et al. 2020; Zellers et al. 2018; Zhang et al. 2019). Although current one-stage methods do not specifically address the long-tail problem, previous studies have reported their results with existing statistical-based unbiased training (e.g., bi-level sampling (Li et al. 2021)) or inference (e.g., logit adjustment (Menon et al. 2020)) methods. We also report our method with statistical-based unbiased methods for further comparison.

Results of Visual Genome The experimental results in Table 1 demonstrate that BCTR achieves superior mR@ performance compared to other baselines. Benefiting from BCG and RFA, BCTR effectively learns balanced feature representations for SGG, significantly improving mR@K by

14% and 21% over SOTA, indicating substantial recall performance improvements across diverse categories. Furthermore, the results for head, body, and tail categories show that BCTR achieves the best performance in the body and tail categories, surpassing the second method by 18% and 67%, respectively. We attribute this excellent performance to RFA, which constrains the feature space, enabling effective learning and representation of tail category features. Our R@K is lower because R@K and mR@K focus on different aspects. Due to the imbalanced VG dataset, R@K emphasizes head predicates with abundant samples, while mR@K favors tail predicates. mR@K is a fairer metric for long-tail datasets as it reduces the influence of dominant relationships (Chang et al. 2021; Desai et al. 2021; Li et al. 2021). Our DETR-based detector struggles with small entity detections, which are prevalent in the VG dataset (Li, Zhang, and He 2022), resulting in lower R@K. Improving small object detection will enhance R@K.

The experimental results in Table 1 further demonstrate that when combined with statistical-based long-tail strategies, our approach achieves the best performance in the body and tail categories compared to other methods. Additionally, our method significantly outperforms existing methods in terms of mR@.

Results of Open Image V6 The experimental results of Open Image V6 are presented in Table 2. These results demonstrate that our approach has significantly enhanced the recall performance of SGG while achieving superior or comparable weighted mAP metrics. Specifically, mR@50 has increased by 6.19, indicating that the SGG tasks benefit from the proposed bidirectional conditioning and random feature alignment.

Table 2: The Results Comparison in Open Image V6

Method	mR@50	R@50	wmAP rel	wmAP phr	score
HOTR(Kim et al. 2021)	40.1	52.7	19.4	21.5	26.9
AS-Net(Chen et al. 2021)	35.2	55.3	25.9	27.5	32.4
SGTR(Li et al. 2022)	42.6	59.9	37.0	38.7	42.3
PGTR(Li et al. 2024)	40.7	62.0	22.7	28.0	30.8
BCTR(ours)	48.8	68.6	36.0	39.0	42.5

Ablation Studies

Model Components The experimental results of the ablation study on the model components are presented in Table 3, which reports the performance of four methods obtained by combining BCG and RFA. In Table 3, models with BCG have 8 decoder layers, while those without BCG have 6. For a fair comparison, we increase the decoder numbers of models without BCG to 8. The results demonstrate that both BCG and RFA contribute to improvements in mR@ and R@. While both modules improve performance across categories with different frequencies, RFA primarily enhances performance in the head and body categories. By combining the two modules, the recall rate of the tail category further improves, resulting in a superior mR@100 performance of 18.4. The ablation studies indicate that BCG and RFA ex-

hibit good compatibility, and integrating the two can further enhance the performance of the SGG task.

Table 3: Ablation Study on Model Components

BCG	RFA	mR@20/50/100	R@20/50/100	H/B/T
✓	✓	8.1/13.7/18.4	20.1/24.8/27.7	27.7/22.0/11.9
	✓	7.9/13.2/17.9	20.4/25.1/28.2	28.1/22.4/10.5
✓		7.7/13.2/17.6	19.9/24.6/27.6	27.2/21.5/10.9
		7.4/12.8/17.0	19.6/24.2/27.3	26.9/21.3/9.7

Feature Interaction Strategy We compare the performance of two different internal message interaction mechanisms, namely Unidirectional Attention (UniAtt) and Bidirectional Attention (BiAtt). For UniAtt, only predicate-to-entity attention is activated. For BiAtt, both entity-to-predicate and predicate-to-entity attention are activated. The experimental results are reported in Table 4, where BiAtt demonstrates better performance than UniAtt, indicating the superiority of the designed Bidirectional Attention mechanism for the SGG task.

Table 4: Ablation Study on Feature Interactions

Method	mR@20/50/100	R@20/50/100	H/B/T
BCG-UniAtt	7.6/13.1/17.5	19.6/24.2/27.3	27.0/21.3/10.8
BCG-BiAtt	7.7/13.2/17.6	19.9/24.6/27.6	27.2/21.5/10.9

Distillation strategy We conduct ablation experiments on distillation strategies to elucidate the effectiveness of the proposed RFA. The results are presented in Table 5, where Trainable Classifier (TC) and Learnable Prompt (LP) (Zhou et al. 2022) represent two CLIP-based classifiers. The results indicate that the performance of both classifiers can be enhanced with Random Feature Alignment. We attribute this improvement to RFA’s ability to align the features of decoders with CLIP while allowing queries to capture other objects/predicates in the image that may not be represented by CLIP. Additionally, the experimental results demonstrate that TC outperforms LP on SGG tasks.

Table 5: Ablation Study on Distillation Strategy

Method	mR@20/50/100	R@20/50/100	H/B/T
TC	7.8/13.0/17.8	20.1/25.1/28.3	28.2/22.4/10.0
TC-RFA	7.8/13.3/18.2	20.4/25.1/28.2	28.1/22.5/10.9
LP	7.5/13.0/17.2	20.1/25.3/28.7	28.4/22.2/8.9
LP-RFA	7.5/13.0/17.6	20.2/25.2/28.3/	28.0/21.9/10.2

Zero-shot Recall The Zero-shot Recall (zR@) of the proposed model is reported in Table 6. zR@ measures the recall of unseen triplets during training, indicating the model’s generalization ability. The experimental results demonstrate that the zR of the model has significantly improved with RFA. Specifically, zR@50/100 has increased by 0.5 and 0.9, respectively, highlighting the effectiveness of VLPs in enhancing downstream task generalization. After combining with BCG, the zR of our method improved to 4.4 and 6.2, outperforming other baselines. This finding aligns with the

observation in Table 3, indicating that the task performance of SGG can be further enhanced by combining BCG and RFA.

Table 6: The Performance of Zero-shot Triplets Retrieval

Method	zR@50/100
BGNN(Li et al. 2021)	0.4/0.9
VCTree-TDE(Tang et al. 2020)	2.6/3.2
SGTR(Li, Zhang, and He 2022)	2.4/5.8
ISGG(Khandelwal and Sigal 2022)	3.9/5.6
SG2JOIT(He et al. 2023)	2.5/3.7
BCTR(ours) w/o BCG+RFA	3.6/5.1
BCTR(ours) w/ RFA	4.1/6.0
BCTR(ours) w/ BCG+RFA	4.4/6.2

Mask Ratio We set α between 0 and 1 to evaluate how the mask ratio affects the model’s performance. The results show high R@K when α is near 0, as the model captures the main content of the image after aligning with CLIP, which accounts for a higher proportion of the VG dataset. As α increases, the model captures more diverse content, improving mR@K. However, when α nears 1, performance decreases due to insufficient feature distillation.

Table 7: Ablation Study on Mask Ratio

Mask Ratio	mR@20/50/100	R@20/50/100	H/B/T
0	7.8/13.0/17.8	20.1/25.1/28.3	28.2/22.4/10.0
0.25	7.8/13.2/17.8	20.2/24.9/27.9	27.8/22.5/10.2
0.5	7.8/13.3/18.2	20.4/25.1/28.2	28.1/22.5/10.9
0.75	7.5/13.3/17.9	20.2/24.8/28.0	28.0/22.4/10.5

Conclusion

In this study, we propose a novel bidirectional conditioning factorization for SGG and implement it by developing an end-to-end SGG model BCTR. BCTR enhances the performance of SGG tasks in two main aspects. First, BCG is designed to facilitate information interaction between entities and predicates through internal bidirectional conditioning and external iterations. Second, RFA is introduced to address the long-tail distribution by aligning the feature space of SGG with a pre-trained visual language model, thereby improving detection performance in tail categories without relying on statistical priors. BCTR has demonstrated superior performance on both the Visual Genome and Open Image V6 datasets.

References

Carion, N.; Massa, F.; Synnaeve, G.; Usunier, N.; Kirillov, A.; and Zagoruyko, S. 2020. End-to-end object detection with transformers. In *European conference on computer vision*, 213–229. Springer.

Chang, X.; Ren, P.; Xu, P.; Li, Z.; Chen, X.; and Hauptmann, A. 2021. A comprehensive survey of scene graphs: Generation and application. *IEEE Transactions on Pattern Analysis and Machine Intelligence*, 45(1): 1–26.

Chen, M.; Liao, Y.; Liu, S.; Chen, Z.; Wang, F.; and Qian, C. 2021. Reformulating hoi detection as adaptive set prediction. In *Proceedings of the IEEE/CVF Conference on Computer Vision and Pattern Recognition*, 9004–9013.

Cong, Y.; Yang, M. Y.; and Rosenhahn, B. 2023. Reltr: Relation transformer for scene graph generation. *IEEE Transactions on Pattern Analysis and Machine Intelligence*.

Desai, A.; Wu, T.-Y.; Tripathi, S.; and Vasconcelos, N. 2021. Learning of visual relations: The devil is in the tails. In *Proceedings of the IEEE/CVF International Conference on Computer Vision*, 15404–15413.

Desai, A.; Wu, T.-Y.; Tripathi, S.; and Vasconcelos, N. 2022. Single-Stage Visual Relationship Learning using Conditional Queries. *Advances in Neural Information Processing Systems*, 35: 13064–13077.

Gan, Z.; Li, L.; Li, C.; Wang, L.; Liu, Z.; Gao, J.; et al. 2022. Vision-language pre-training: Basics, recent advances, and future trends. *Foundations and Trends® in Computer Graphics and Vision*, 14(3–4): 163–352.

Gu, J.; Zhao, H.; Lin, Z.; Li, S.; Cai, J.; and Ling, M. 2019. Scene graph generation with external knowledge and image reconstruction. In *Proceedings of the IEEE/CVF conference on computer vision and pattern recognition*, 1969–1978.

Hayder, Z.; and He, X. 2024. DSGG: Dense Relation Transformer for an End-to-end Scene Graph Generation. In *Proceedings of the IEEE/CVF Conference on Computer Vision and Pattern Recognition*, 28317–28326.

He, T.; Gao, L.; Song, J.; and Li, Y.-F. 2023. Toward a Unified Transformer-Based Framework for Scene Graph Generation and Human-Object Interaction Detection. *IEEE Transactions on Image Processing*, 32: 6274–6288.

Im, J.; Nam, J.; Park, N.; Lee, H.; and Park, S. 2024. Egtr: Extracting graph from transformer for scene graph generation. In *Proceedings of the IEEE/CVF Conference on Computer Vision and Pattern Recognition*, 24229–24238.

Johnson, J.; Krishna, R.; Stark, M.; Li, L.-J.; Shamma, D.; Bernstein, M.; and Fei-Fei, L. 2015. Image retrieval using scene graphs. In *Proceedings of the IEEE conference on computer vision and pattern recognition*, 3668–3678.

Khandelwal, S.; and Sigal, L. 2022. Iterative scene graph generation. *Advances in Neural Information Processing Systems*, 35: 24295–24308.

Kim, B.; Lee, J.; Kang, J.; Kim, E.-S.; and Kim, H. J. 2021. Hotr: End-to-end human-object interaction detection with transformers. In *Proceedings of the IEEE/CVF Conference on Computer Vision and Pattern Recognition*, 74–83.

Kim, H.; Kim, S.; Ahn, D.; Lee, J. T.; and Ko, B. C. 2024. Scene Graph Generation Strategy with Co-occurrence Knowledge and Learnable Term Frequency. *arXiv preprint arXiv:2405.12648*.

Krishna, R.; Zhu, Y.; Groth, O.; Johnson, J.; Hata, K.; Kravitz, J.; Chen, S.; Kalantidis, Y.; Li, L.-J.; Shamma, D. A.; et al. 2017. Visual genome: Connecting language and vision using crowdsourced dense image annotations. *International journal of computer vision*, 123: 32–73.

- Kundu, S.; and Aakur, S. N. 2023. IS-GGT: Iterative Scene Graph Generation With Generative Transformers. In *Proceedings of the IEEE/CVF Conference on Computer Vision and Pattern Recognition*, 6292–6301.
- Kuznetsova, A.; Rom, H.; Alldrin, N.; Uijlings, J.; Krasin, I.; Pont-Tuset, J.; Kamali, S.; Popov, S.; Mallocci, M.; Kolesnikov, A.; et al. 2020. The open images dataset v4: Unified image classification, object detection, and visual relationship detection at scale. *International Journal of Computer Vision*, 128(7): 1956–1981.
- Li, R.; Zhang, S.; and He, X. 2022. Sgtr: End-to-end scene graph generation with transformer. In *proceedings of the IEEE/CVF conference on computer vision and pattern recognition*, 19486–19496.
- Li, R.; Zhang, S.; Lin, D.; Chen, K.; and He, X. 2024. From Pixels to Graphs: Open-Vocabulary Scene Graph Generation with Vision-Language Models. In *Proceedings of the IEEE/CVF Conference on Computer Vision and Pattern Recognition*, 28076–28086.
- Li, R.; Zhang, S.; Wan, B.; and He, X. 2021. Bipartite graph network with adaptive message passing for unbiased scene graph generation. In *Proceedings of the IEEE/CVF Conference on Computer Vision and Pattern Recognition*, 11109–11119.
- Li, Y.; Ouyang, W.; Wang, X.; and Tang, X. 2017. Vip-cnn: Visual phrase guided convolutional neural network. In *Proceedings of the IEEE conference on computer vision and pattern recognition*, 1347–1356.
- Liao, Y.; Zhang, A.; Lu, M.; Wang, Y.; Li, X.; and Liu, S. 2022. Gen-vlkt: Simplify association and enhance interaction understanding for hoi detection. In *Proceedings of the IEEE/CVF Conference on Computer Vision and Pattern Recognition*, 20123–20132.
- Lin, B.; Zhu, Y.; and Liang, X. 2022. Atom correlation based graph propagation for scene graph generation. *Pattern Recognition*, 122: 108300.
- Liu, H.; Yan, N.; Mortazavi, M.; and Bhanu, B. 2021. Fully convolutional scene graph generation. In *Proceedings of the IEEE/CVF Conference on Computer Vision and Pattern Recognition*, 11546–11556.
- Lu, C.; Krishna, R.; Bernstein, M.; and Fei-Fei, L. 2016. Visual relationship detection with language priors. In *Computer Vision–ECCV 2016: 14th European Conference, Amsterdam, The Netherlands, October 11–14, 2016, Proceedings, Part I 14*, 852–869. Springer.
- Menon, A. K.; Jayasumana, S.; Rawat, A. S.; Jain, H.; Veit, A.; and Kumar, S. 2020. Long-tail learning via logit adjustment. *arXiv preprint arXiv:2007.07314*.
- Shi, J.; Zhang, H.; and Li, J. 2019. Explainable and explicit visual reasoning over scene graphs. In *Proceedings of the IEEE/CVF conference on computer vision and pattern recognition*, 8376–8384.
- Shit, S.; Koner, R.; Wittmann, B.; Paetzold, J.; Ezhov, I.; Li, H.; Pan, J.; Sharifzadeh, S.; Kaissis, G.; Tresp, V.; et al. 2022. Relationformer: A unified framework for image-to-graph generation. In *European Conference on Computer Vision*, 422–439. Springer.
- Sun, P.; Zhang, R.; Jiang, Y.; Kong, T.; Xu, C.; Zhan, W.; Tomizuka, M.; Li, L.; Yuan, Z.; Wang, C.; et al. 2021. Sparse r-cnn: End-to-end object detection with learnable proposals. In *Proceedings of the IEEE/CVF conference on computer vision and pattern recognition*, 14454–14463.
- Tang, K.; Niu, Y.; Huang, J.; Shi, J.; and Zhang, H. 2020. Unbiased scene graph generation from biased training. In *Proceedings of the IEEE/CVF conference on computer vision and pattern recognition*, 3716–3725.
- Tang, K.; Zhang, H.; Wu, B.; Luo, W.; and Liu, W. 2019. Learning to compose dynamic tree structures for visual contexts. In *Proceedings of the IEEE/CVF conference on computer vision and pattern recognition*, 6619–6628.
- Teng, Y.; and Wang, L. 2022. Structured sparse r-cnn for direct scene graph generation. In *Proceedings of the IEEE/CVF Conference on Computer Vision and Pattern Recognition*, 19437–19446.
- Xu, D.; Zhu, Y.; Choy, C. B.; and Fei-Fei, L. 2017. Scene graph generation by iterative message passing. In *Proceedings of the IEEE conference on computer vision and pattern recognition*, 5410–5419.
- Yang, X.; Tang, K.; Zhang, H.; and Cai, J. 2019. Auto-encoding scene graphs for image captioning. In *Proceedings of the IEEE/CVF conference on computer vision and pattern recognition*, 10685–10694.
- Yin, G.; Sheng, L.; Liu, B.; Yu, N.; Wang, X.; Shao, J.; and Loy, C. C. 2018. Zoom-net: Mining deep feature interactions for visual relationship recognition. In *Proceedings of the European conference on computer vision (ECCV)*, 322–338.
- Yu, R.; Li, A.; Morariu, V. I.; and Davis, L. S. 2017. Visual relationship detection with internal and external linguistic knowledge distillation. In *Proceedings of the IEEE international conference on computer vision*, 1974–1982.
- Zareian, A.; Wang, Z.; You, H.; and Chang, S.-F. 2020. Learning visual commonsense for robust scene graph generation. In *Computer Vision–ECCV 2020: 16th European Conference, Glasgow, UK, August 23–28, 2020, Proceedings, Part XXIII 16*, 642–657. Springer.
- Zellers, R.; Yatskar, M.; Thomson, S.; and Choi, Y. 2018. Neural motifs: Scene graph parsing with global context. In *Proceedings of the IEEE conference on computer vision and pattern recognition*, 5831–5840.
- Zhan, Y.; Yu, J.; Yu, T.; and Tao, D. 2019. On exploring undetermined relationships for visual relationship detection. In *Proceedings of the IEEE/CVF Conference on Computer Vision and Pattern Recognition*, 5128–5137.
- Zhang, J.; Shih, K. J.; Elgammal, A.; Tao, A.; and Catanzaro, B. 2019. Graphical contrastive losses for scene graph parsing. In *Proceedings of the IEEE/CVF Conference on Computer Vision and Pattern Recognition*, 11535–11543.
- Zhou, K.; Yang, J.; Loy, C. C.; and Liu, Z. 2022. Learning to prompt for vision-language models. *International Journal of Computer Vision*, 130(9): 2337–2348.
- Zhu, G.; Zhang, L.; Jiang, Y.; Dang, Y.; Hou, H.; Shen, P.; Feng, M.; Zhao, X.; Miao, Q.; Shah, S. A. A.; et al. 2022. Scene graph generation: A comprehensive survey. *arXiv preprint arXiv:2201.00443*.